PAPER

Check for updates

Lead calix[n]arenes (n = 4, 6, 8): structures and ring opening homo-/co-polymerization capability for cyclic esters†

Tian Xing, Timothy J. Prior [ID] and Carl Redshaw [ID] *

Reaction of [LiPb(O*i*Pr)$_3$]$_2$ (generated *in situ*) with either *p-tert*-butylcalix[4]areneH$_4$ (L^{4}H$_4$) or *p-tert*-butyl-calix[6]areneH$_6$ (L^{6}H$_6$) resulted in the heterometallic lithium/lead complexes [Pb$_4$Li$_2$(L^4)$_4$H$_6$(MeCN)$_3$]·4.5MeCN (**1**·4.5MeCN) and [Pb$_8$Li$_{10}$Cl$_2$(L^{6}H$_2$)$_3$(L^6)(OH)$_2$(O)$_2$(H$_2$O)$_2$(MeCN)$_4$]·14MeCN (**2**·14MeCN), respectively. Use of the dimethyleneoxa-bridged *p-tert*-butyltetrahomodioxacalix[6]areneH$_6$ (L$^6'$H$_6$) with five equivalents of [Pb(O*i*Pr)$_2$] afforded [Pb$_{13}$(L$^6'$)$_3$O$_4$(*i*PrOH)]·11MeCN (**3**·11MeCN). Use of the larger *p-tert*-butylcalix[8]-areneH$_8$ (L^{8}H$_8$) with [Pb(O*t*Bu)$_2$] or {Pb[N(TMS)$_2$]} (TMS = SiMe$_3$) afforded the products [Pb$_{12}$(L^8)$_2$O$_4$]·8.7C$_7$H$_8$ (**4**·8.7C$_7$H$_8$) or [Pb$_6$(SiMe$_3$)$_2$(L^8)O$_2$Cl$_2$] (**5**), respectively. Reaction of {Pb[N(TMS)$_2$]} (generated *in situ* from (Me$_3$Si)$_2$NH, *n*BuLi and PbCl$_2$) with L^{6}H$_6$ afforded, after work-up (MeCN), the mixed-metal complex [Pb$_{10}$Li$_2$(L^6)$_2$(OH)Cl(O)$_4$]·9.5MeCN (**6**·9.5MeCN). Reaction of distilled {Pb[N(TMS)$_2$]} (six equivalents) with L^{8}H$_8$ resulted in the complex [Pb$_{12}$(L^8)$_2$O$_4$]·12MeCN (**7**·12MeCN). Complexes **1–7**, Pb(O*i*Pr)$_2$ and [Pb(N(TMS)$_2$)$_2$] have been screened for their potential to act as pre-catalysts in the ring opening polymer-ization (ROP) of ε-caprolactone (ε-CL) and δ-valerolactone (δ-VL) and the copolymerization thereof. Generally, the lithiated complexes **1** and **2** exhibited better activities than the other pre-catalysts screened herein. For ε-CL and δ-VL, moderate activity at 130 °C over 24 h was observed for **1–7**. In the case of the co-polymerization of ε-CL with δ-VL, **1–7**, Pb(O*i*Pr)$_2$ and [Pb(N(TMS)$_2$)$_2$] afforded reasonable conversions and high molecular weight polymers. The systems **1–7**, Pb(O*i*Pr)$_2$ and [Pb(N(TMS)$_2$)$_2$] also proved to be active in the ROP of the *rac*-lactide (*r*-LA); the activity trend was found to be **1** > **2** ≈ Pb(O*i*Pr)$_2$ ≈ [Pb (N(TMS)$_2$)$_2$] > **4** > **5** ≈ **6** ≈ **7** > **3**.

Introduction

The ring opening polymerization (ROP) of cyclic esters is attracting much attention in light of the current environmental issues with petroleum-derived plastics.[1] As seen in previous work, coordination chemistry can play a crucial role in the development of new greener polymers with desirable features, given that control over the ligands at the metal centre of the catalyst employed for ROP can allow for control over the resultant polymer properties.[2] Ideally, the metal centre needs to be highly active, as well as abundant and non-toxic, however sometimes it is necessary for one of these criteria to become secondary if one or more of the others is exemplary. With this in mind, we note the elegant work by Sarazin *et al.* reporting

that for main group elements of group IV, systems employing the ligand set 2-CH$_2$NR$_2$-4,6-*t*Bu$_2$-C$_6$H$_2$OH, {LO^i}H, (i = 1, NR$_2$ = N((CH$_2$)$_2$OCH$_3$)$_2$; i = 2, NR$_2$ = NEt$_2$; i = 3, NR$_2$ = aza-15-crown-5) were ROP active. The ROP activity followed the trend Ge^{II} ≪ Sn^{II} ≪ Pb^{II},[3] whilst for a subsequent report on [M(μ$_2$-O*i*Pr)$_2$]$_n$, the trend was Ge ≪ Sn < Pb.[4] Thus, despite the issue of toxicity associated with lead compounds, and given our interest in metallocalix[n]arenes as ROP catalysts,[5] combined with a lack of lead calixarenes,[6] this work has utilized the calix[n]arenes shown in Chart 1, which differ in both size (n = 4, 6, 8) and/or bridge (–CH$_2$– or –CH$_2$OCH$_2$–), to access new lead-containing calix[n]arene complexes. We note that a number of lead complexes derived from carboxylated calixarenes have been reported.[7] Moreover, the coordination chemistry of calix[n] arenes, where n ≥ 6, is somewhat limited.[8] A number of interesting multi-metallic species (see Chart 2) have been structurally characterized. The ability of these complexes to act as catalysts for the ROP of ε-caprolactone (ε-CL), δ-valerolactone (δ-VL) and *rac*-lactide (*r*-LA) has been investigated; the copolymerization of ε-CL and δ-VL was also investigated.

Plastics Collaboratory, Department of Chemistry, University of Hull, Cottingham Road, Hull, HU6 7RX, UK. E-mail: c.redshaw@hull.ac.uk
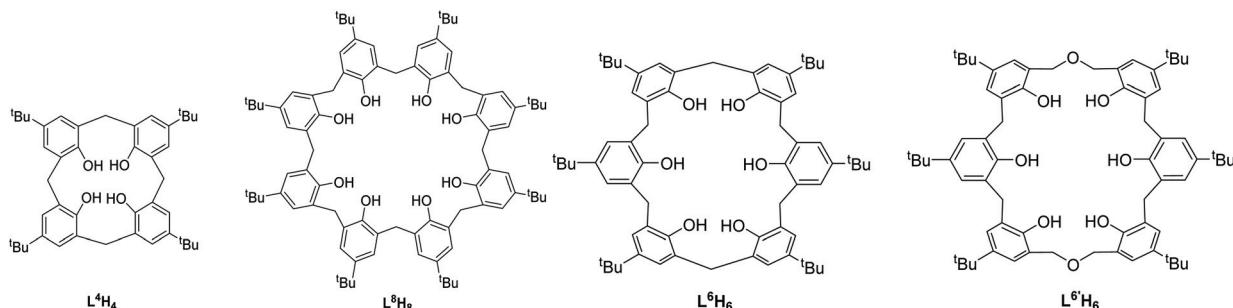
**Chart 1** The calixarenes employed herein.
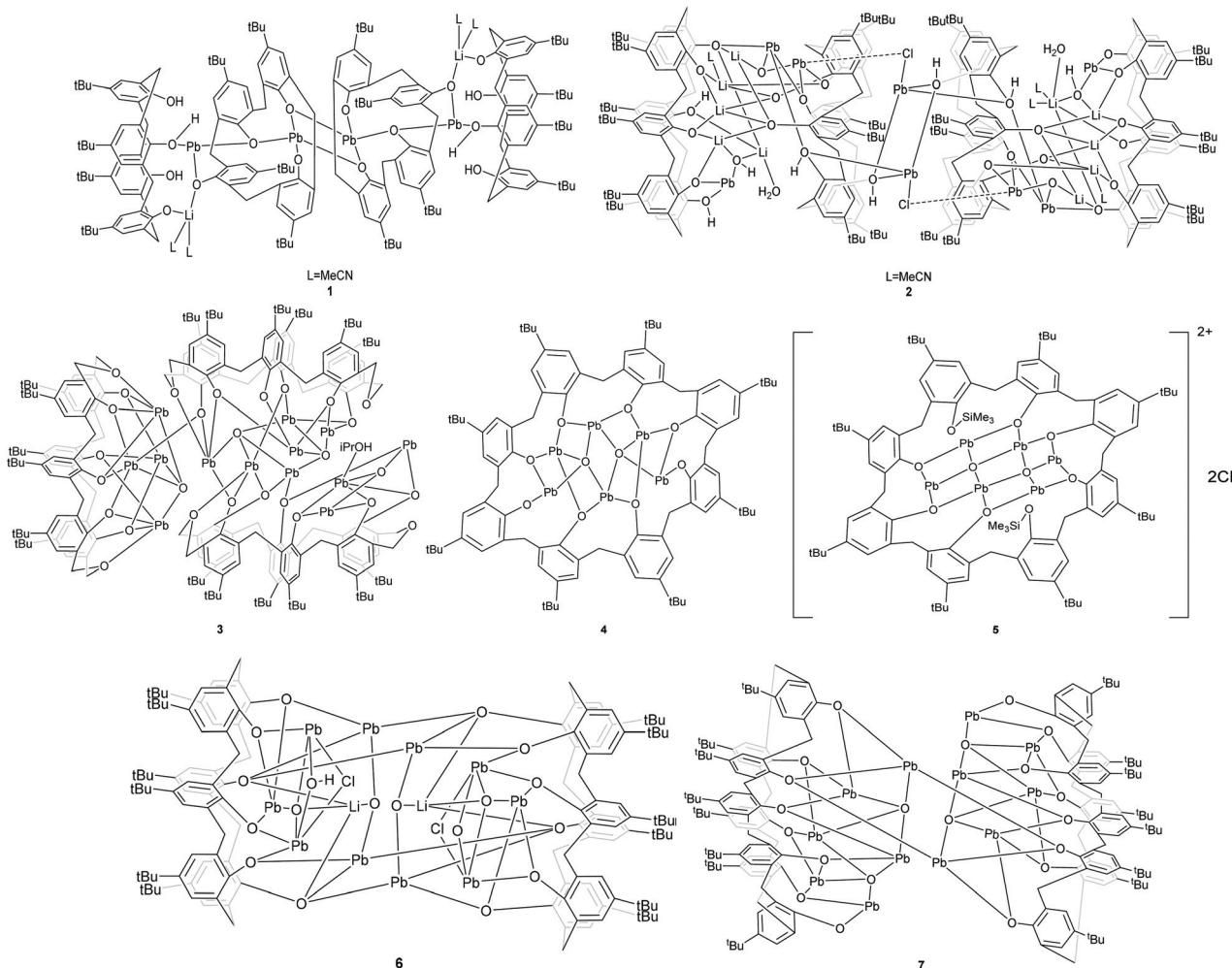
Chart 2 Lead calix[*n*]arenes reported herein.

Results and discussion

Syntheses and solid-state structures

Given that we have previously found the metallocalix[*n*]arenes generated from *in situ* heterobimetallic reagents of the form Li[M(OR)$_x$] (M = Cr, Fe) tend to be highly crystalline,[9] we selected here as our entry point the reagent [LiPb(O*i*Pr)$_3$]$_2$, which was prepared by the addition of LiO*i*Pr to *in situ* generated [Pb(O*i*Pr)$_2$] (from PbCl$_2$, (TMS)$_2$NH, *n*BuLi and *i*PrOH; TMS = trimethylsilyl). We note that the Sarazin *et al.* preparation of [LiPb(μ$_2$-O*t*Bu)$_3$(μ$_3$-O*t*Bu)]$_2$ initially isolates [Pb(μ$_2$-O*t*Bu)$_2$]$_3$ prior to the addition of LiO*t*Bu.[4] Subsequent reaction of our *in situ* generated precursor with one equivalent of *p-tert*-butylcalix[4]areneH$_4$ (L^{4}H$_4$) in refluxing toluene led, following

work-up (extraction into acetonitrile), to the complex $[Pb_4Li_2(L^4)_4H_6(MeCN)_3]\cdot4.5MeCN$ (**1**·4.5MeCN) in moderate yield (37%). The molecular structure of **1**·4.5MeCN is shown in Fig. 1, with selected bond lengths and angles given in the caption. For crystallographic data, see Table S1 (ESI†). The cluster is centrosymmetric and contains four Pb atoms and two lithiums. At the centre of the cluster are two Pb atoms (Pb2) and two oxygen atoms (O2) from a calix[4]arene in a diamond formation (Fig. 1 bottom). On either side of this lie calix[4]arene molecules that are twisted so that one of the aromatic rings points downwards from the bowl of the calixarene; this enables it to bind Pb2 on one side and Pb1 on the other. There is a further calix[4]arene at each end of the cluster (in bowl configuration) and this forms one O–Pb bond to Pb1. The Pb–O bond lengths [2.235(5)–2.528(6) Å] are somewhat longer than those found in the thiacalix[4]arene (L^{4S}) complexes $\{Pb[L^{4S}(Obenzyl)_2]\}$ (2.149(2) Å) and $\{Pb[L^{4S}(OTMS)_2]\}$ (2.1632(18)/2.1891(19) Å),[6b] and in the aryloxides [(BDI)Pb(Ar)] (2.182(4)/2.212(2) Å; Ar = 2,6-tBu-4-MeC_6H_2, BDI = [{N(2,6-iPr$_2C_6H_3$)C(Me)}$_2$CH]) and [Pb(OAr)$_2$] (2.211(2)/2.228(2) Å; Ar = C_6H_3-2.6-(C_6H_3-2,6-iPr$_2$).[10b] The longer bond lengths in **1** and in the other structures herein reflect the bridging modes adopted by the Pb centres. The lithium ions are coordinated by one oxygen from each of the two calixarenes; coordination about the Li is completed by MeCN. In essence, the complex can be described as a cluster of four stacked calix[4]arene molecules threaded by an LiOPbOPb(μ_2-O)PbOPbOLi chain.

Using a similar method to **1**, but using p-tert-butylcalix[6]areneH$_6$ (L^6H_6) led to the isolation of the complex $[Pb_8Li_{10}Cl_2(L^6H_2)_3(L^6)(OH)_2(O)_2(H_2O)_2(MeCN)_4]\cdot14MeCN$ (**2**·14MeCN) in moderate yield (47%). The molecular structure of **2**·14MeCN is shown in Fig. 2, with selected bond lengths and angles given in the caption. The cluster is reasonably close to being centrosymmetric and is composed of four calixarenes that bind 8 lead ions and 10 lithium ions. At the centre of the cluster there is a Pb_2O_2 diamond which is linked to further lead atoms via bridging chloride ions. Two further Pb ions are bound near the plane of the six oxygen atoms by each calixarene adjacent to the centre. One more Pb is bound on

each side by the terminal calixarenes, which also binds 5 lithium ions. There are additional oxide and hydroxide anions between the Pb and Li ions and bound acetonitrile. The presence of the oxo ligands is thought to be due to adventitious hydrolysis.

Use of the precursors [Pb(OR)$_2$] (R = iPr or tBu) or {Pb[N(TMS)$_2$]} also allows access to metallocalix[n]arene species. Indeed, interaction of five equivalents of [Pb(OiPr)$_2$] with p-tert-butyltetrahomodioxacalix[6]areneH$_6$ ($L^{6'}H_6$) afforded, following work-up, the complex $[Pb_{13}(L^{6'})_3O_4(iPrOH)]\cdot11MeCN$ (**3**·11MeCN). We note that use of dioxamethylene-bridged calixarenes can be beneficial for certain polymerization processes.[11] The molecular structure of **3**·11MeCN is shown in Fig. 3, with selected bond lengths and angles given in the caption. The complex is a large cluster of 13 unique Pb atoms composed of two smaller clusters. A pair of calixarenes are arranged roughly on top of each other. Between these lie nine lead atoms (Pb5–Pb13), and four oxide anions (O26–O29). Each lead is coordinated by the oxygen atoms of the calixarene and the oxide. Uniquely, the coordination of Pb11 is completed by an isopropoxide. The second part of the cluster is approximately perpendicular to the first and linked to it through the bond Pb2–O9. This contains four lead atoms (Pb1–Pb4) which surround a central oxide (O25). Around the cluster there are 11 unbound molecules of MeCN, some of which are ordered, others located by SQUEEZE.

Similar use of [Pb(OtBu)$_2$], but with p-tert-butylcalix[8]areneH$_8$ (L^8H_8) afforded the colourless dimer $[Pb_{12}(L^8)_2O_4]\cdot8.7C_7H_8$ (**4**·8.7C$_7$H$_8$). The molecular structure of half of the dimer of **4**·8.7MeCN is shown in Fig. 4, with selected bond lengths and angles given in the caption. In each half dimer, a hexanuclear lead cluster (Fig. 4, right) sits on the open face of an L^8 bowl. The μ_4-oxo centres are thought to arise via the presence of adventitious hydrolysis. Two Pb–aryl interactions present result in the formation of the observed dimers (see Fig. S1, ESI†). In solution, we only see (by [207]Pb NMR spectroscopy) two distinct lead environments (see Experimental section).
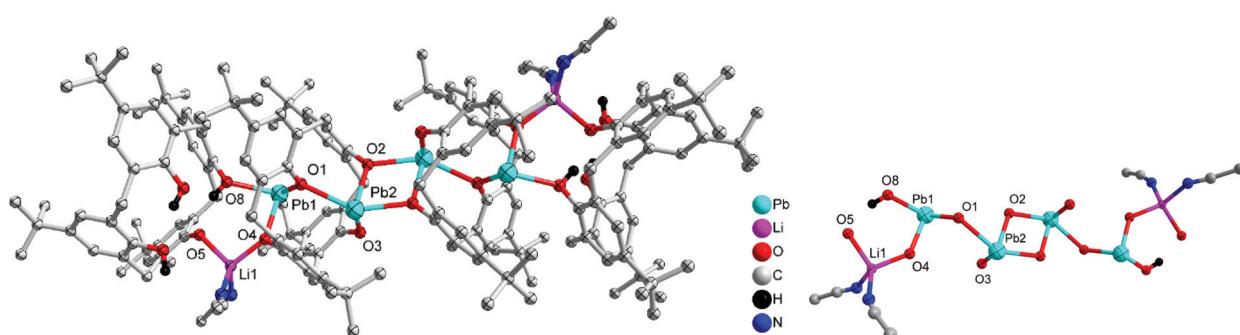
Fig. 1 Molecular structure and core of $[Pb_4Li_2(L^4)_4H_6(MeCN)_3]\cdot4.5MeCN$ (**1**·4.5MeCN). Non coordinated solvent molecules have been removed for clarity. Selected bond lengths (Å) and angles (°): Pb(1)–O(1) 2.235(5), Pb(1)–O(4) 2.260(6), Pb(1)–O(8) 2.357(6), Pb(2)–O(1) 2.528(6), Pb(2)–O(2) 2.283(6), O(1)–Pb(1)–O(4) 82.7(2), O(1)–Pb(1)–O8 101.3(2), O(4)–Pb(1)–O(8) 81.5(2), O(2)–Pb(2)–O(1) 77.74(19), O(3)–Pb(2)–O(1) 98.7(2), O(4)–Li(1)–O(5) 102.4(8), O(4)–Li(1)–N(2) 126.5(11), O(4)–Li(1)–N(1) 102.9(10), O(5)–Li(1)–N(1) 121.2(12).
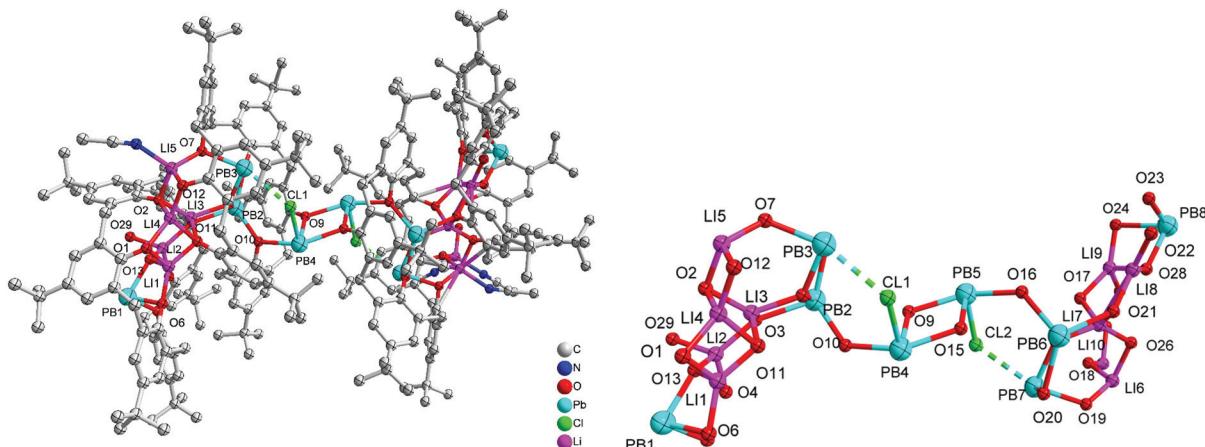
Fig. 2 Molecular structure and core of [Pb$_8$Li$_{10}$Cl$_2$(L^{6}H$_2$)$_3$(L^6)(OH)$_2$(O)$_2$(H$_2$O)$_2$(MeCN)$_4$]·14MeCN (2·14MeCN). Selected bond lengths (Å) and angles (°): O(1)−Li(1) 2.063(16), O(1)−Li(4) 1.964(17), O(2)−Li(3) 1.978(15), O(2)−Li(4) 1.960(17), O(2)−Li(5) 1.943(16), O(3)−Pb(2) 2.496(6), O(3)−Li(2) 2.064(19), O(5)−Pb(1) 2.266(6), O(6)−Pb(1) 2.288(6), O(7)−Pb(3) 2.318(5), O(8)−Pb(3) 2.313(6), O(9)−Pb(4) 2.280(6), O(9)−Pb(5) 2.467(6), O(10)−Pb(2) 2.342(6), O(10)−Pb(4) 2.390(6), Li(4)−O(2)−Li(3) 81.2(6), Li(5)−O(2)−Li(3) 105.2(6), Li(5)−O(2)−Li(4) 83.2(7), Li(2)−O(3)−Pb(2) 157.1(6), Li(3)−O(3)−Pb(2) 93.9(5), Li(3)−O(3)−Li(2) 95.1(7), Pb(3)−O(8)−Pb(2) 104.7(2), Li(5)−O(7)−Pb(3) 122.3(5).
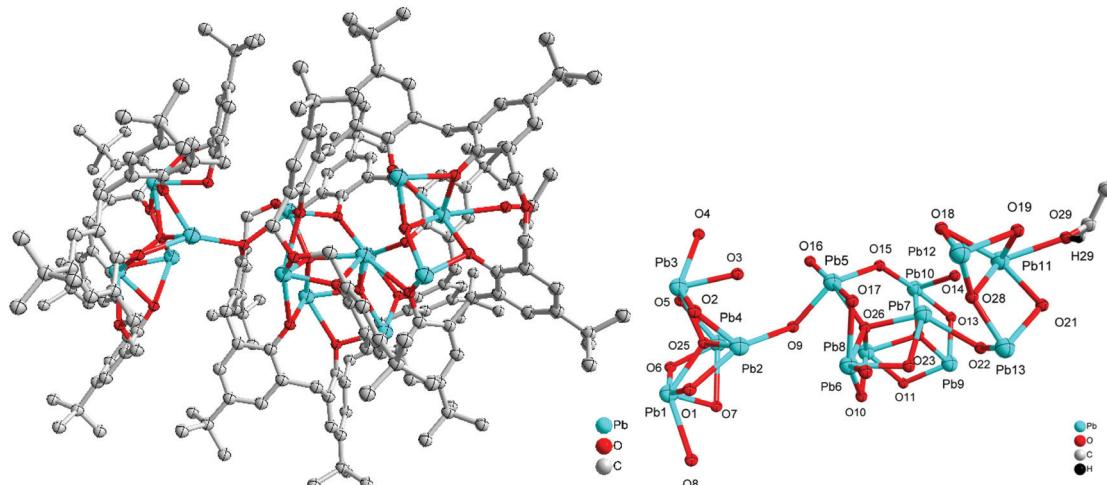
**Fig. 3** Molecular structure and core of [Pb$_{13}$(L$^{6'}$)$_3$O$_4$(iPrOH)]·11MeCN (3·11MeCN). Selected bond lengths (Å) and angles (°): Pb(1)−Pb(2) 3.6746(6), Pb(1)−O(1) 2.356(8), Pb(1)−O(6) 2.553(8), Pb(1)−O(7) 2.359(8), Pb(2)−Pb(3) 3.5012(7), Pb(2)−O(1) 2.405(8), Pb(2)−O(2) 2.224(9), Pb(2)−O(9) 2.738(8), Pb(3)−O(2) 2.483(8), Pb(3)−O(3) 2.340(9), Pb(3)−O(4) 2.757(9), Pb(3)−O(5) 2.365(9), Pb(4)−O(5) 2.379(10), Pb(4)−O(6) 2.208(8), Pb(4)−O(7) 2.751(8), Pb(5)−O(9) 2.447(7), Pb(5)−O(15) 2.503(8), Pb(5)−O(16) 2.586(7), Pb(6)−O(17) 2.581(7), Pb(6)−O(23) 2.251(7), Pb(7)−Pb(10) 3.5418(6), O(1)−Pb(1)−Pb(2) 39.97(19), O(1)−Pb(1)−Pb(4) 108.51(19), O(1)−Pb(1)−O(6) 145.6(2), O(1)−Pb(1)−O(7) 106.6(3), Pb(5)−O(9)−Pb(2) 118.6(3), O(1)−Pb(2)−Pb(1) 38.99(19), O(1)−Pb(2)−O(9) 149.7(3), O(2)−Pb(2)−O(1) 76.6(3), O(2)−Pb(2)−O(9) 128.1(3), O(3)−Pb(3)−O(2) 68.7(3), O(5)−Pb(3)−O(4) 70.5(3), O(5)−Pb(4)−O(7) 132.0(3), O(9)−Pb(5)−O(15) 127.1(3).

The same calix[8]arene, namely L^{8}H$_8$, on interaction with {Pb[N(TMS)$_2$]} (TMS = SiMe$_3$) afforded after, work-up (MeCN), the product [Pb$_6$(SiMe$_3$)$_2$(L^8)O$_2$Cl$_2$] (5). The complex is a centrosymmetric Pb cluster that contains a single calix[8] arene. The asymmetric unit contains one half of the calixarene, three Pb ions and one oxide. The molecular structure of 5 is shown in Fig. 5, with selected bond lengths and angles given in the caption. Two of the phenols of the calixarene on opposite sides of the ring carry SiMe$_3$ groups and do not bind

to a metal. At the centre of the ring there is a cluster with composition Pb$_6$O$_2$ that is formed from two edge-sharing OPb$_4$ tetrahedra (oxide surrounded by four Pb ions). The coordination about the Pb ions is completed by the oxygen atoms of the calixarene. Pb1 sits at the apex of a square pyramid; the other unique Pb ions are three coordinate.

Furthermore, the precursor {Pb[N(TMS)$_2$]}, generated *in situ* from (Me$_3$Si)$_2$NH, *n*BuLi and PbCl$_2$, was treated with L^{6}H$_6$. Following work-up (MeCN), the complex [Pb$_{10}$Li$_2$(L^6)$_2$(OH)Cl
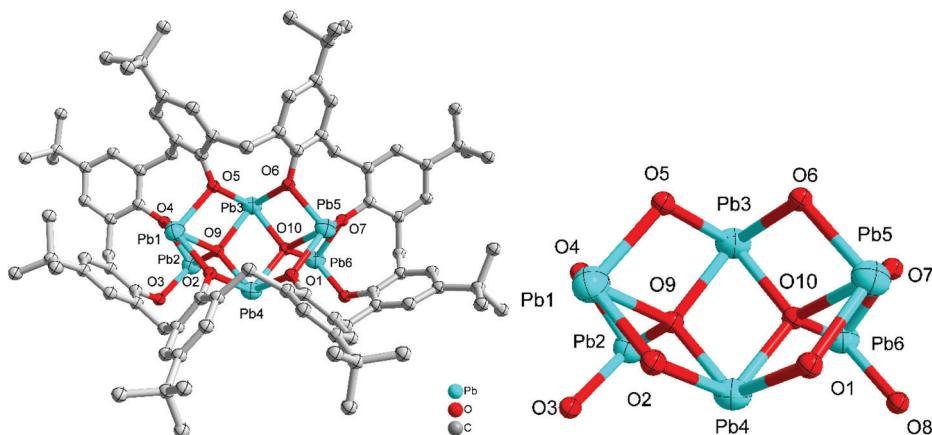
Fig. 4 Molecular structure and core of $[Pb_{12}(L^8)_2O_4]\cdot8.7C_7H_8$ ($4\cdot8.7C_7H_8$). Selected bond lengths (Å) and angles (°): Pb(1)−O(9) 2.297(4), Pb(1)−O(5) 2.336(5), Pb(1)−O(2) 2.419(5), Pb(1)−O(4) 2.432(5), Pb(2)−O(3) 2.206(4), Pb(2)−O(9) 2.268(5), Pb(2)−O(4) 2.287(4), Pb(3)−O(5) 2.258(4), Pb(3)−O(10) 2.317(4), Pb(3)−O(6) 2.341(4), Pb(3)−O(9) 2.350(4), O(9)−Pb(1)−O(2) 69.91(15), O(5)−Pb(1)−O(2) 101.56(17), O(9)−Pb(1)−O(4) 68.63(16), O(3)−Pb(2)−O(9) 91.99(16), O(3)−Pb(2)−O(4) 90.09(17), O(9)−Pb(2)−O(4) 71.73(16), O(5)−Pb(3)−O(6) 79.54(16), O(10)−Pb(3)−O(6) 71.26(15), O(5)−Pb(3)−O(9) 73.37(16).
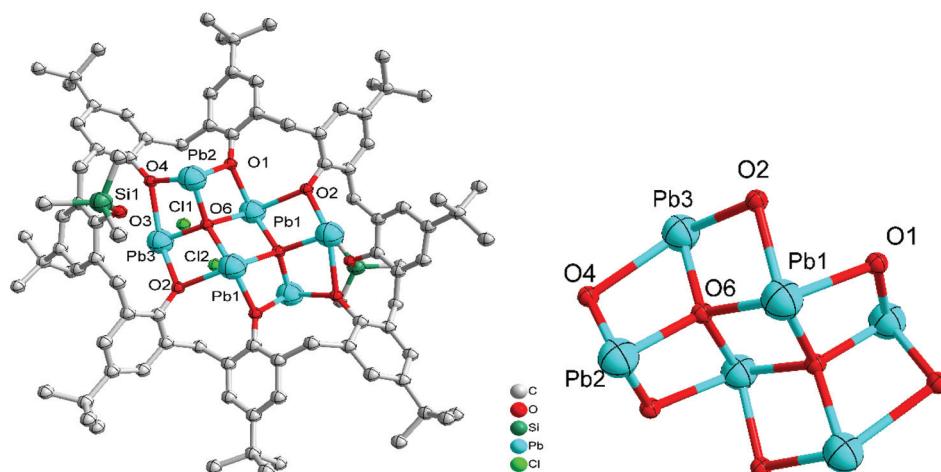

Fig. 5 Molecular structure and core of $[Pb_6(SiMe_3)_2(L^8)O_2Cl_2]$ (**5**). Selected bond lengths (Å) and angles (°): O(1)−Pb(1) 2.416(12), O(1)−Pb(2) 2.244(13), O(2)−Pb(1) 2.485(13), O(2)−Pb(3) 2.442(12), O(3)−Si(1) 1.729(14), O(4)−Pb(2) 2.249(11), O(4)−Pb(3) 2.678(11), Pb(1)−O(6) 2.369(10), Pb(2)−O(6) 2.236(10), Pb(3)−O(6) 2.227(10), Pb(2)−O(1)−Pb(1) 104.9(4), Pb(3)−O(2)−Pb(1) 100.9(4), Pb(2)−O(4)−Pb(3) 95.8(4), O(1)−Pb(1)−O(2) 76.4(4), O(6)−Pb(1)−O(1) 120.3(4), O(6)−Pb(1)−O(2) 72.2(4), O(2)−Pb(3)−O(4) 131.7(4), O(6)−Pb(3)−O(2) 75.4(4), Pb(2)−O(6)−Pb(1) 114.8(5), Pb(3)−O(6)−Pb(1) 111.5(4), Pb(3)−O(6)−Pb(2) 110.5(4).

$(O)_4]\cdot9.5MeCN$ ($6\cdot9.5MeCN$) was isolated. The molecular structure of $6\cdot9.5MeCN$ is shown in Fig. 6, with selected bond lengths and angles given in the caption. The compound features a centrosymmetric cluster comprised of two symmetry-equivalent parts. Each calixarene binds one lithium ion and five lead ions, but between these ions there are oxide anions surrounded by four metal ions. In addition, there are hydroxide and chloride bridging between two lead ions (each 50% occupied and sharing a site). The two calixarenes do not lie face-on in the solid state but one is translated related to the other so that the bonding holing the $Pb_{10}Li_2$ cluster together is

two pairs of Pb–O(calix) bonds; hydroxide and oxide are not involved in bridging.

Finally, to avoid any possible chloride or lithium contamination, freshly distilled $\{Pb[N(TMS)_2]\}$ was reacted with L^8H_8. Work-up led to the isolation of the colourless complex $[Pb_{12}(L^8)_2O_4]\cdot12MeCN$ ($7\cdot12MeCN$) in 31% isolated yield. A view of the molecular structure is shown in Fig. 7, with selected bond lengths and angles given in the caption. The asymmetric unit of $7\cdot12MeCN$ contains two independent molecules each comprising one L^8H_8-derived ligand and five Pb ions (Pb1 to Pb5 in first molecule and the rest
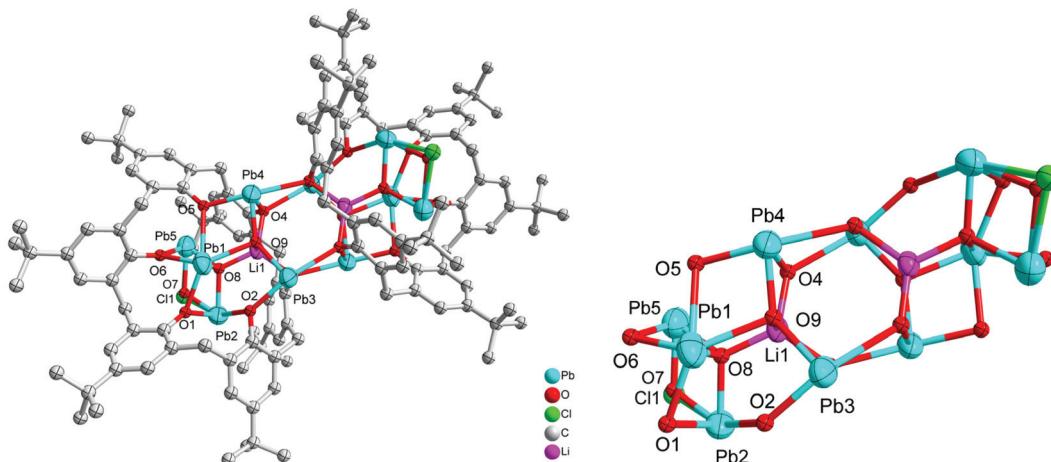
Fig. 6 Molecular structure and core of $[Pb_{10}Li_2(L^6)_2(OH)Cl(O)_4]\cdot9.5MeCN$ (**6**·9.5MeCN). Selected bond lengths (Å) and angles (°): Pb(3)−O(9) 2.158(3), Pb(3)−O(4) 2.728(3), Pb(3)−O(3) 2.392(3), Pb(3)−O(2) 2.306(3), Pb(5)−Cl(1) 2.669(4), Pb(4)−O(9) 2.159(3), Pb(4)−O(4) 2.428(3), Pb(4)−O(3) 2.719(3), Pb(4)−O(5) 2.313(3), O(9)−Pb(4)−O(4) 79.83(11), O(9)−Pb(4)−O(3) 99.61(10), O(9)−Pb(4)−O(5) 84.26(10), O(9)−Pb(4)−Li(1) 40.34(19), O(4)−Pb(4)−O(3) 70.32(9), O(8)−Pb(1)−O(1) 73.17(11), O(8)−Pb(1)−O(6) 74.46(10), O(6)−Pb(1)−O(1) 72.49(10), O(6)−Pb(1)−O(1) 72.49(10), O(8)−Pb(2)−O(1) 77.32(11), O(8)−Pb(2)−Li(1) 29.17(15), O(8)−Pb(2)−O(7) 72.2(3).
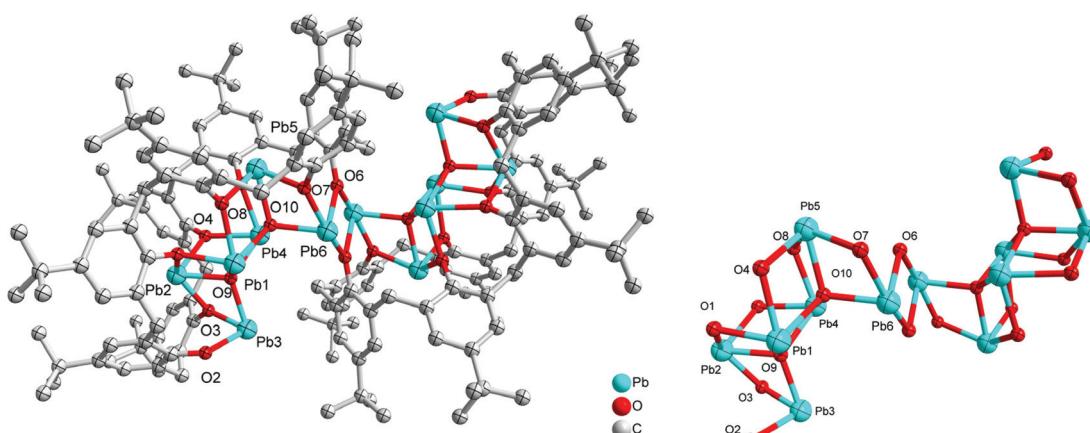
Fig. 7 Molecular structure and core of $[Pb_{12}(L^8)_2O_4]\cdot12MeCN$ (**7**·12MeCN). For clarity, hydrogen atoms and solvent molecules are not shown. Selected bond lengths (Å) and angles (°): Pb(4)−O(10) 2.356(6), Pb(4)−O(9) 2.335(6), Pb(4)−O(5) 2.278(6), Pb(4)−O(4) 2.370(6), Pb(2)−O(9) 2.247(6), Pb(2)−O(3)−−2.454(7), Pb(2)−O(4) 2.287(6), Pb(2)−O(1) 2.388(7), Pb(6)−O(6) 2.664(7), Pb(1)−O(10) 2.281(6), Pb(1)−O(9) 2.374(7), Pb(1)−O(8) 2.419(7), Pb(5)−O(10) 2.275(6), Pb(5)−O(5) 2.421(6), Pb(3)−O(9) 2.269(7), Pb(3)−O(2) 2.192(7), O(10)−Pb(4)−O(4) 119.7(2), O(9)−Pb(4)−O(10) 74.4(2), O(9)−Pb(4)−O(4) 72.3(2), O(5)−Pb(4)−O(10) 70.0(2), O(5)−Pb(4)−O(9) 111.7(2), O(9)−Pb(2)−O(3) 71.1(2), O(9)−Pb(2)−O(4) 75.5(2), O(4)−Pb(2)−O(3) 80.8(2), O(10)−Pb(1)−O(9) 75.1(2).

five Pb ion in second molecule. This is a centrosymmetric dimer bridged by the Pb_2O_2 square.

Ring opening polymerization studies

General. The performance of these complexes to act as catalysts for the ring opening polymerization (ROP) of ε-caprolactone (ε-CL, Table 1), δ-valerolactone (δ-VL, Table 2), the co-polymerization of ε-caprolactone and δ-valerolactone (Table 3) and *rac*-lactide (*r*-LA, Table 4) has been investigated. Results are compared *versus* the precursors Pb(O*i*Pr)$_2$, and [Pb(N(TMS)$_2$)$_2$].

ε-Caprolactone (ε-CL)

Complexes **1–7**, Pb(O*i*Pr)$_2$, and [Pb(N(TMS)$_2$)$_2$] were screened for their ability to polymerise ε-caprolactone and the results are collated in Table 1. The polymerization screening indicated that the best conditions were 500 equivalents of ε-caprolactone to metal at a temperature of 130 °C. Complex **1** was also active at low catalyst loading leading to *ca*. 54% conversion after 8 h for 1000 equivalents of monomer. All polymers obtained were of low polydispersity (PDI < 2), which suggested that these polymerizations occurred without significant

Table 1 ROP of ε-CL using **1–7**, Pb(O*i*Pr)$_2$, and [Pb(N(TMS)$_2$)$_2$]

Run	Cat.	CL : Pb : BnOH	$T/^\circ$C	t (h)	Conv^a (%)	$M_{n,GPC} \times 10^{-3\,b}$	$M_w \times 10^{-3\,b}$	$M_{n,cal} \times 10^{-3\,c}$	PDI^d	TON^f
1	**1**	1000 : 1 : 1	130	8	54.2	8.05	15.34	61.86	1.91	542
2	**1**	500 : 1 : 1	130	8	60.4	8.49	14.55	34.47	1.71	302
3	**1**	250 : 1 : 1	130	8	57.3	6.52	9.45	16.35	1.45	143
4	**1**	100 : 1 : 1	130	8	52.4	3.56	5.14	5.98	1.44	52
5	**1**	500 : 1 : 1	100	8	35.4	4.38	5.79	20.20	1.32	177
6	**1**	500 : 1 : 1	80	8	24.8	1.23	1.43	14.15	1.16	124
7	**1**^{e}	500 : 1 : 1	130	8	49.1	3.22	5.42	28.02	1.69	246
8	**2**	500 : 1 : 1	130	8	72.6	8.94	11.57	41.43	1.29	363
9	**3**	500 : 1 : 1	130	8	55.2	6.72	8.09	31.50	1.20	276
10	**4**	500 : 1 : 1	130	8	40.7	2.95	3.57	23.23	1.21	204
11	**5**	500 : 1 : 1	130	8	49.1	3.75	4.50	28.02	1.20	246
12	**6**	500 : 1 : 1	130	8	42.0	3.89	5.12	23.97	1.32	210
13	**7**	500 : 1 : 1	130	8	35.8	3.12	4.37	20.43	1.40	179
14	Pb(O*i*Pr)$_2$	500 : 1 : 1	130	8	24.9	—	—	—	—	124
15	[Pb(N(TMS)$_2$)$_2$]	500 : 1 : 1	130	8	15.8	—	—	—	—	79
16	**1**	500 : 1 : 1	130	24	70.5	10.59	14.24	40.24	1.34	353
17	**2**	500 : 1 : 1	130	24	92.1	11.25	12.45	52.56	1.11	461
18	**3**	500 : 1 : 1	130	24	66.9	6.81	8.06	38.18	1.18	335
19	**4**	500 : 1 : 1	130	24	59.4	4.20	4.81	33.90	1.15	297
20	**5**	500 : 1 : 1	130	24	62.6	5.11	6.09	35.73	1.19	313
21	**6**	500 : 1 : 1	130	24	65.8	4.89	5.25	37.55	1.07	329
22	**7**	500 : 1 : 1	130	24	49.8	4.01	5.32	28.42	1.33	249
23	Pb(O*i*Pr)$_2$	500 : 1 : 1	130	24	33.8	1.35	1.56	19.29	1.16	169
24	[Pb(N(TMS)$_2$)$_2$]	500 : 1 : 1	130	24	27.1	1.24	1.74	15.47	1.40	135
25	**1**	500 : 1 : 0	130	24	44.7	8.33	8.73	25.51	1.05	224
26	**2**	500 : 1 : 0	130	24	72.4	5.23	6.98	41.32	1.33	362
27	**3**	500 : 1 : 0	130	24	58.1	3.21	4.53	33.16	1.41	291
28	**4**	500 : 1 : 0	130	24	35.2	2.51	3.70	20.09	1.47	176
29	**5**	500 : 1 : 0	130	24	52.8	2.86	4.21	30.13	1.47	264
30	**6**	500 : 1 : 0	130	24	36.0	2.54	4.65	20.55	1.83	180
31	**7**	500 : 1 : 0	130	24	36.4	2.86	3.27	20.77	1.14	182
32	Pb(O*i*Pr)$_2$	500 : 1 : 0	130	24	28.4	0.56	0.82	16.21	1.46	142
33	[Pb(N(TMS)$_2$)$_2$]	500 : 1 : 0	130	24	19.6	0.72	1.25	11.19	1.74	98

^{a} Determined by ^{1}H NMR spectroscopy. ^{b} $M_{n/w}$, GPC values corrected considering Mark–Houwink factor (0.56) from polystyrene standards in THF. ^{c} Calculated from ([monomer]$_0$/Pb) × conv (%) × monomer molecular weight (M_{CL} = 114.14) + molecular weight of BnOH. ^{d} From GPC. ^{e} Reaction performed in air. ^{f} Turnover number (TON) = number of moles of ε-CL consumed/number of moles Pb.

Table 2 ROP of δ-VL using **1–7**, Pb(O*i*Pr)$_2$, and [Pb(N(TMS)$_2$)$_2$]

Run	Cat.	VL : Pb : BnOH	$T/^\circ$C	t (h)	Conv^a (%)	$M_{n,GPC} \times 10^{-3\,b}$	$M_w \times 10^{-3\,b}$	$M_{n,cal} \times 10^{-3\,c}$	PDI^d	TON^f
1	**1**	1000 : 1 : 1	130	8	61.2	7.53	12.57	61.29	1.67	612
2	**1**	500 : 1 : 1	130	8	68.9	7.90	12.87	34.50	1.63	345
3	**1**	250 : 1 : 1	130	8	61.0	5.12	8.56	15.27	1.67	153
4	**1**	100 : 1 : 1	130	8	55.5	2.52	3.96	5.56	1.57	56
5	**1**	500 : 1 : 1	100	8	41.2	3.49	7.12	20.63	2.04	206
6	**1**	500 : 1 : 1	80	8	31.5	—	—	—	—	158
7	**1**^{e}	500 : 1 : 1	130	8	43.1	4.01	6.54	21.58	1.63	216
8	**2**	500 : 1 : 1	130	8	75.9	10.98	13.83	38.00	1.26	380
9	**3**	500 : 1 : 1	130	8	52.4	5.32	6.00	26.24	1.13	262
10	**4**	500 : 1 : 1	130	8	36.2	2.15	2.65	18.13	1.23	181
11	**5**	500 : 1 : 1	130	8	34.3	1.97	2.38	17.18	1.20	172
12	**6**	500 : 1 : 1	130	8	37.8	2.23	4.02	18.92	1.80	189
13	**7**	500 : 1 : 1	130	8	30.1	1.54	2.86	15.07	1.86	176
14	Pb(O*i*Pr)$_2$	500 : 1 : 1	130	8	26.2	—	—	—	—	131
15	[Pb(N(TMS)$_2$)$_2$]	500 : 1 : 1	130	8	14.2	—	—	—	—	71

^{a} Determined by ^{1}H NMR spectroscopy. ^{b} $M_{n/w}$, GPC values corrected considering Mark–Houwink factor (0.57) from polystyrene standards in THF. ^{c} Calculated from ([monomer]$_0$/Pb) × conv (%) × monomer molecular weight (M_{VL} = 100.16) + molecular weight of BnOH. ^{d} From GPC. ^{e} Reaction performed in air. ^{f} Turnover number (TON) = number of moles of δ-VL consumed/number of moles Pb.

side reactions. Interestingly, complex **1** proved to be active also under aerobic conditions achieving *ca*. 49% conversion over 8 h (Table 1, run 7).

The screening of complexes **1–7**, Pb(O*i*Pr)$_2$, and [Pb (N(TMS)$_2$)$_2$] (Table 1) revealed that the lead/lithium-based complexes **1** and **2** exhibited higher activities than other complexes

Table 3 ROP of co-polymer (ε-CL + δ-VL) using 1–7

Run	Cat	CL : VL : Pb : BnOH	T/°C	CL : VL[a]	Conv[b] (%)	$M_{n,GPC} \times 10^{-3}$ [c]	$M_w \times 10^{-3}$ [c]	PDI[d]
1	1[e]	250 : 250 : 1 : 1	130	42 : 58	61.0	10.98	13.83	1.26
2	2[e]	250 : 250 : 1 : 1	130	50 : 50	68.4	11.10	15.97	1.44
3	3[e]	250 : 250 : 1 : 1	130	52 : 48	52.6	6.97	8.69	1.25
4	4[e]	250 : 250 : 1 : 1	130	45 : 55	53.1	5.60	8.37	1.50
5	5[e]	250 : 250 : 1 : 1	130	43 : 57	47.2	4.56	6.89	1.51
6	5[f]	250 : 250 : 1 : 1	130	64 : 36	53.9	6.16	7.56	1.23
7	5[g]	250 : 250 : 1 : 1	130	49 : 51	46.2	3.96	5.89	1.49
8	6[e]	250 : 250 : 1 : 1	130	45 : 55	39.2	4.55	6.24	1.37
9	7[e]	250 : 250 : 1 : 1	130	46 : 54	28.4	2.95	4.78	1.62

[a] Ratio of ε-CL to δ-VL observed in the co-polymer by ^{1}H NMR spectroscopy. [b] Determined by ^{1}H NMR spectroscopy. [c] $M_{n/w}$, GPC values corrected considering Mark–Houwink method from polystyrene standards in THF, $M_{n/w}$ GPC = $[0.56 \times M_{n/w \text{ measured}} \times (1 - \%CL) + 0.57 \times M_{n/w}$ measured $\times (1 - \%VL)] \times 10^3$. [d] From GPC. [e] ε-Caprolactone was firstly added for 24 h, then δ-valerolactone was added and heating for 24 h. [f] δ-Valerolactone was firstly added for 24 h, then ε-caprolactone was added and heating for 24 h. [g] ε-Caprolactone and δ-valerolactone were added at the same time and heating for 24 h.

**Table 4** ROP of *rac*-lactide using complexes 1–7, Pb(O*i*Pr)$_2$, and [Pb(N(TMS)$_2$)$_2$]

Run	Cat.	LA : Pb : BnOH	T/°C	t (h)	Conv[a] (%)	$M_{n,GPC} \times 10^{-3}$ [b]	$M_w \times 10^{-3}$ [b]	P_r [c]	$M_{n,cal} \times 10^{-3}$ [d]	PDI[e]	TON[f]
1	1	500 : 1 : 1	130	24	64.3	5.33	9.01	0.45	46.40	1.69	322
2	2	500 : 1 : 1	130	24	56.2	6.82	14.51	0.61	40.57	2.13	281
3	3	500 : 1 : 1	130	24	24.9	1.45	2.46	0.52	18.04	1.70	125
4	4	500 : 1 : 1	130	24	34.9	1.64	3.05	0.39	25.24	1.86	175
5	5	500 : 1 : 1	130	24	30.5	1.63	2.76	0.55	22.07	1.69	153
6	6	500 : 1 : 1	130	24	35.8	2.14	3.89	0.51	25.80	1.82	179
7	7	500 : 1 : 1	130	24	31.6	1.83	3.44	0.49	22.77	1.88	158
8	Pb(O*i*Pr)$_2$	500 : 1 : 1	130	24	54.7	5.45	8.45	0.52	31.22	1.55	273
9	[Pb(N(TMS)$_2$)$_2$]	500 : 1 : 1	130	24	52.4	3.92	4.60	0.55	29.90	1.17	262

[a] Determined by ^{1}H NMR spectroscopy on crude reaction mixture. [b] $M_{n/w}$, GPC values corrected considering Mark–Houwink factor (0.58) from polystyrene standards in THF. [c] From 2D *J*-resolved ^{1}H NMR spectroscopy. [d] Calculated from ([monomer]$_0$/Pb) × conv. (%) × monomer molecular weight (M_{LA} = 144.13) + molecular weight of BnOH. [e] From GPC. [f] Turnover number (TON) = number of moles of *rac*-lactide consumed/number of moles Pb.

under the conditions employed herein. After 24 h (Table 1), complexes 3–7 afforded relatively lower conversions (<70%), whereas higher conversions (>70%) were reached using complexes 1 and 2, under similar conditions. The higher conversions achieved using 1 and 2 may be attributed to the presence of the lithium centers, although it should be noted that the lability of the MeCN ligands present in these species may also prove beneficial. This is in line with our recent study on titano-

calix[4]arenes, in which the presence of a labile ligand (*i.e.* MeCN and H$_2$O) proved beneficial for the catalyst activity.[12] From a kinetic study (Fig. 8), it was observed that the PCL polymerization rate followed the order: 2 > 1 > 3 > 4 ≈ 5 ≈ 6 > 7 (with first order dependence, see Kinetics section). In general, compared with the larger lead-calix[8]arene complexes 4, 5 and 7, those derived from calix[4 or 6]arenes, *i.e.* 1–3, were found to be relatively more active (Table 1, runs 16–18). This is
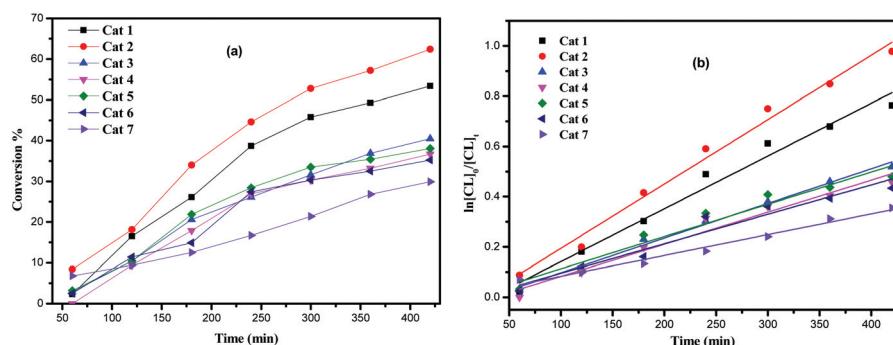
Fig. 8 (a) Relationship between conversion and time for the polymerization of ε-CL by using complex 1–7; (b) plot of ln[CL]$_0$/[CL]$_t$ *vs.* time for the polymerization of ε-CL by using complexes 1–7; conditions: T = 130 °C, $n_{monomer}$: n_{Pb} : BnOH = 500 : 1 : 1.

similar to the situation observed for a series of tungstocalix[6 and 8]arenes and lithium-containing calix[6 and 8]arenes, where use of L^8-derived complexes was detrimental for the ROP of cyclic esters.[13,14] Indeed, results for the lead calixarene systems herein are comparable with those of the lithium calix[6 and 8]arenes under similar conditions (130 °C, 24 h, 500 : 1 : 1); conversions for the latter are in the range 35–81%. An aluminium/lithium system was found to be more active (98%).[14] Furthermore, compared with **4** and **5**, the higher activity of **3** was thought to be due to the higher flexibility of the –CH₂OCH₂– bridge allowing better access to the active centre(s) and/or to the stabilization of the active species by the oxygen atoms of said bridge.[11] The precursors Pb(OiPr)₂, and [Pb(N(TMS)₂)₂] were far less effective for the ring polymerization of ε-CL (runs 14/15, 23/24, 32/33). Based on the results in Table 1 (runs 16–24), the activity trend was found to be **2** > **1** > **3** > **4** ≈ **5** ≈ **6** > **7** > Pb(OiPr)₂ > [Pb(N(TMS)₂)₂]. The MALDI-ToF mass spectra (*e.g.* Fig. S2, ESI†) indicated the presence of a BnO end group, which agrees with the ¹H NMR spectra of the PCL (*e.g.* Fig. S3, ESI†) and indicates that the polymerization proceeded *via* a coordination insertion mechanism. Indeed, the MALDI-ToF spectrum of the sample displayed a major series of peaks separated by 114 *m/z* units accountable to two OH terminated PCL *n*-mers [M = 17 (OH) + 1(H) + n × 114.14 (CL) + 22.99 (Na⁺)]. Additionally, there is a family of peaks consistent with the polymer terminated by OH and BnO end groups [M = n × 114.12 (CL) + 108.05 (BnOH) + 22.99 (Na⁺)].

δ-Valerolactone (δ-VL)

Complexes **1–7**, Pb(OiPr)₂, and [Pb(N(TMS)₂)₂] were also evaluated as catalysts, in the presence of one equivalent of BnOH, for the ROP of δ-VL (Table 2). Using **1**, the conditions of temperature and [Pb] : [δ-VL] ratio were varied. On increasing the temperature to 130 °C and lowering the monomer to catalyst ratio, best observed results were achieved at 130 °C using [V] : [δ-VL] at 1 : 500 over 8 h. As in the case of the ROP of ε-CL, kinetic studies (Fig. 9) revealed that the catalytic activities followed the order: **2** > **1** > **3** > **4** ≈ **5** ≈ **6** ≈ **7** > Pb(OiPr)₂ > [Pb(N(TMS)₂)₂]. The systems **1** and **2** (runs 2 and 8, Table 2), which contain the smaller calix[4 or 6]arenes, outperform lithiated calix[6 and 8]arenes under similar conditions

(500 : 1 : 1, 130 °C, 8 h); the conversions for the latter are 33–55%. An aluminium/lithium system was found to be more active (89%).[14]

As for the ROP of ε-Cl, there was evidence of significant transesterification and nearly all observed M_n values were significantly lower than the calculated values. The MALDI-ToF mass spectra (Fig. S4, ESI†) exhibited a major family of peaks consistent with BnO end groups [M = 108.05 (BnOH) + n × 100.12 (VL) + 22.99 (Na⁺)], and a family assigned to the PVL with two OH end groups [M = 17 (OH) + 1(H) + n × 114.14 (CL) + 22.99 (Na⁺)]. ¹H NMR spectra of the PVL also indicated the presence of an BnO end group (*e.g.* Fig. S5, ESI†).

Co-polymerization of ε-CL and δ-VL

The complexes exhibited moderate conversions, with the mixed-metal complex **2** performing best (68.4%). Under the conditions employed, the systems **2**, **3** and **5** showed a preference for CL incorporation (50–64%), and in the case of **5**, this was despite the initial addition of δ-VL. Complex **1** exhibited the highest preference (58%) for VL incorporation. In general, the systems appeared to be relatively well behaved with PDIs in the range 1.23–1.62; ¹H NMR spectra were consistent with the presence of BnO and OH end groups (Fig. S6, ESI†). The composition of the copolymer was further investigated by ¹³C NMR spectroscopy. In fact, diagnostic resonances belonging to CL–VL, CL–CL, VL–VL and VL–CL dyads can be observed in the region between δ 63.73 and 64.35 ppm (Fig. S7, ESI†). Based on the current results, the number-average sequence length was found to be 1.35 and 3.09 for CL and VL, respectively, consistent with a randomness degree R of 0.98, which suggests the copolymers possess a "blocking" tendency (Fig. S7, eqn (S1)–(S3), ESI†).[15]

ROP of *rac*-lactide

Selected complexes were also employed, in combination with BnOH, as catalysts in the ROP of *r*-LA (Table 4). Best conversion was achieved in the presence of **1** (64.3%, run 1). The M_n of the polymer was lower than the calculated value albeit with narrow molecular weight distribution (5330 and 1.69, respectively). In the case of systems **1–7**, all polymers obtained were of relatively low polydispersity (PDI < 2.13), which suggested that
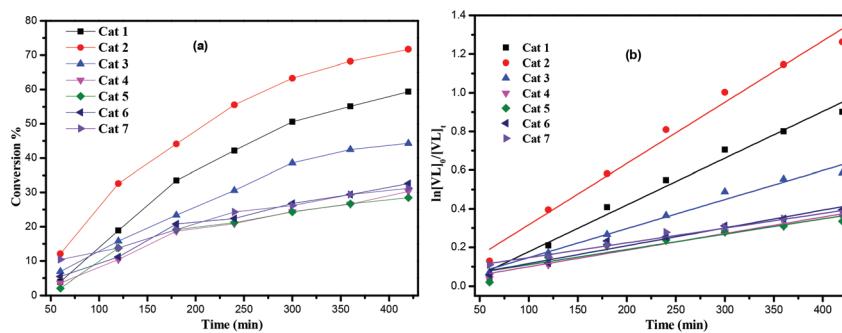

Fig. 9 (a) Relationship between conversion and time for the polymerization of δ-VL by using complex **1–7**; (b) plot of ln[VL]₀/[VL]$_t$ *vs.* time for the polymerization of δ-VL by using complexes **1–7**; conditions: T = 130 °C, $n_{monomer}$: n_{Pb} : BnOH = 500 : 1 : 1.
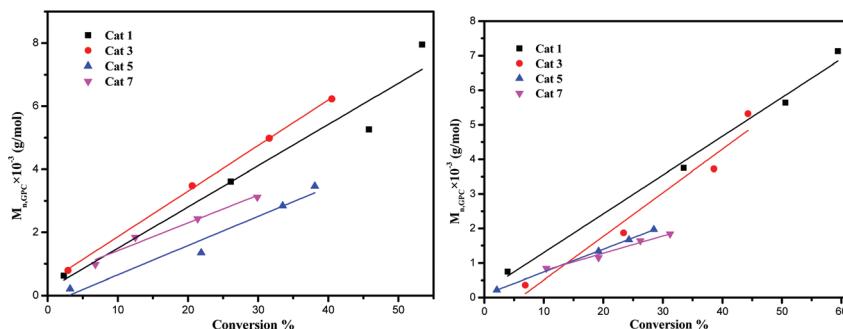
Fig. 10 Left: M_n vs. monomer conversion in the ROP of ε-CL by using **1**, **3**, **5** and **7**; right: M_n vs. monomer conversion in the ROP of δ-VL by using **1**, **3**, **5** and **7**; conditions: T = 130 °C, $n_{monomer} : n_{Pb} : BnOH = 500 : 1 : 1$.

there was reasonable control for polymerization. However, **3** only allowed for *ca.* 25% monomer conversion affording low molecular weight species. Interestingly, compared with ε-CL and δ-VL, both Pb(O*i*Pr)$_2$, and [Pb(N(TMS)$_2$)$_2$] exhibited better performances for the ROP of *r*-LA (runs 8 and 9), whereas surprisingly the dioxacalix[6]arene-derived system performed the worst in terms of conversion. Conversions, PDIs and TONs were comparable with the best performing lead calixarenes. Moreover, the lead calixarenes were found to be comparable with lithium-based calix[6 and 8]arenes (23–55% conversion) under the same conditions (500 : 1 : 1, 130 °C, 24 h), with **1** exhibiting a slightly higher conversion than an aluminium/lithium calix[8]arene (62%).[14] Based on the results in Table 4 (runs 1–9), it was observed that the PLA polymerization conversion rate followed the order: **1** > **2** ≈ Pb(O*i*Pr)$_2$ ≈ [Pb(N(TMS)$_2$)$_2$] > **4** > **5** ≈ **6** ≈ **7** > **3**. ^{1}H NMR spectra of the PLA indicated the presence of a BnO end group (*e.g.* Fig. S8, ESI†), which agrees with the MALDI-ToF mass spectra (*e.g.* Fig. S9, ESI†). The sample was analysed by MALDI-ToF mass spectra in positive-linear mode, the expected series corresponding to repeating unit mass of 72/144 for half/full LA was observed and the polymer chain was terminated by OH and BnO end group [M = 108.05 (BnOH) + n × 72.06 (C$_3$H$_4$O$_2$) + 22.99 (Na$^+$)]. The syndiotactic bias was determined by 2D *J*-resolved ^{1}H NMR spectroscopy, investigating the methine area (5.13–5.20 ppm) of the spectra (*e.g.* figure. S10, ESI†).[16] The peaks were assigned to the corresponding tetrads according to the literature.[17] For *rac*-lactide, when P_r = 0.5, the afforded PLA is an atactic polymer, and when P_r = 0, an isotactic polymer. The observed values herein (P_r = 0.39–0.61) suggested the catalysts afforded almost heterotactic polymers.

Kinetics

From a kinetic study of the ROP of ε-CL using **1–7**, it was observed that the polymerization rate exhibited first-order dependence on the ε-CL concentration (Fig. 8), and the conversion of monomer achieved over 420 min was >20%. The activity trend in this case revealed that **2** was the most active followed by **1** > **3** > **4** ≈ **5** ≈ **6** > **7**. An induction period of the first 2 h was observed for complexes **1–7**, which could be ascribed to the longer time required for the formation of the

catalytically active species. A similar result was also observed for the polymerization of δ-VL (Fig. 9).

The dependence of the M_n and molecular weight distribution on the monomer conversion in the reactions catalyzed by **1**, **3**, **5** and **7** with BnOH was also investigated (Fig. 10). For the ROP of ε-CL, the polymer M_n was shown to increase linearly with the conversion, which suggested that the polymerization was well controlled (Fig. 10, left). A similar outcome was also observed in the reaction involving δ-VL (Fig. 10, right).

Conclusions

In conclusion, the use of the precursors [LiPb(O*i*Pr)$_3$], Pb(O*i*Pr)$_2$, Pb(O*t*Bu)$_2$ or Pb(N(TMS)$_2$)$_2$, on interaction with a series of calix[*n*]arenes (*n* = 4, 6, 8) allowed access to a number of rather complicated lead compounds (see Chart 2). The molecular structures reveal how these macrocycles can support multiple metal centres, which adopt some interesting structural motifs. Complex **1–7** proved active in the ring opening homo-/co-polymerization of ε-caprolactone (ε-CL) and δ-valerolactone (δ-VL) under the conditions employed, and the activity trend was found to be **2** > **1** > **3** > **4** ≈ **5** ≈ **6** > **7** > Pb(O*i*Pr)$_2$ > [Pb(N(TMS)$_2$)$_2$]; first order kinetics were observed for the ROP of ε-CL and δ-VL. The NMR spectroscopy and mass spectrometry (MALDI-ToF) characterization of selected polymer samples suggested the formation of linear PCLs and PVLs ended by –BnO and –OH groups. The catalysts **1–7** also be proved to be active in the ROP of the *rac*-lactide (*r*-LA), the activity trend was found to be **1** > **2** ≈ Pb(O*i*Pr)$_2$ ≈ [Pb(N(TMS)$_2$)$_2$] > **4** > **5** ≈ **6** ≈ **7** > **3**, affording near heterotactic polymers.

Experimental

General

All reactions were conducted under an inert atmosphere using standard Schlenk techniques. Toluene and hexane was dried from sodium, acetonitrile was distilled from calcium hydride, diethylether was distilled from sodium benzophenone, and all

solvents were degassed prior to use. The dioxacalix[6]arene,[18] [LiPb(OiPr)$_3$],[4] [Pb(N(TMS)$_2$)$_2$],[19] Pb(OiPr)$_2$ and Pb(OtBu)$_2$[20] were prepared according to the literature methods. All other chemicals were purchased from commercial sources. IR spectra (nujol mulls, KBr or NaCl windows) were recorded on a Nicolet Avatar 360 FT IR spectrometer; ^{1}H NMR spectra were recorded at room temperature on a Varian VXR 400 S spectrometer at 400 MHz or a Gemini 300 NMR spectrometer or a Bruker Advance DPX-300 spectrometer at 300 MHz. The ^{1}H NMR spectra were calibrated against the residual protio impurity of the deuterated solvent. Elemental analyses were performed by the elemental analysis service at the University of Hull. Matrix Assisted Laser Desorption/Ionization Time of Flight (MALDI-TOF) mass spectrometry was performed in a Bruker autoflex III smart beam in linear mode, and the spectra were acquired by averaging at least 100 laser shots. 2,5-Dihydroxybenzoic acid was used as the matrix and THF as solvent. Sodium chloride was dissolved in methanol and used as the ionizing agent. Samples were prepared by mixing 20 μl of matrix solution in THF (2 mg mL^{-1}) with 20 μL of matrix solution (10 mg mL^{-1}) and 1 μL of a solution of ionizing agent (1 mg mL^{-1}). Then 1 mL of these mixtures was deposited on a target plate and allowed to dry in air at ambient temperature.

Preparation of [Pb$_4$Li$_2$(L^4)$_4$H$_6$(MeCN)$_3$]·4.5MeCN (1·4.5MeCN)

L^{4}H$_4$ (1.00 g, 1.54 mmol) and [LiPb(OiPr)$_3$] (0.63 g, 1.57 mmol), generated *in situ* from PbCl$_2$ and LiOiPr, were combined in toluene (20 mL) and the system was refluxed for 12 h. On cooling, the volatiles were removed *in vacuo*, and the residue was extracted into MeCN (20 mL). On standing at 0 °C for 2 days, colourless prisms formed. Yield, 0.53 g, 37%. Anal. calcd for C$_{182}$H$_{223}$Li$_2$N$_3$O$_{17}$Pb$_4$ (sample dried *in vacuo* for 12 h, −4.5MeCN): C, 61.28; H, 6.30; N, 1.18%; found C, 61.40; H, 6.25%; N, 1.51%; IR (nujol mull, KBr): 2726w, 2263w, 1607w, 1460s, 1377s, 1304m, 1280m, 1260s, 1204m, 1125m, 1093m, 1018m, 914w, 872m, 818s, 795s. ^{1}H NMR (CDCl$_3$) δ: 10.33 (s, 6H, −OH), 6.98–7.48 (m, 32H, aryl$H$), 4.42–4.38 (m, 4H, −CH$_2$), 4.24 (d, J = 14 Hz, 12H, −CH$_2$−), 3.83–3.89 (m, 4H, −CH$_2$−), 3.48 (d, J = 14 Hz, 12H, −CH$_2$−), 1.96 (s, 12H, MeCN), 1.13–1.36 (m, 144H, −C(CH$_3$)$_3$). ^{7}Li (CDCl$_3$) δ: 3.61(bs). ^{207}Pb NMR (C$_6$D$_6$) δ: −2392 (s), −3401 (s). Mass Spec (EI): 1761 ([M − 7.5MeCN]/2 + 2Na$^+$).

Preparation of [Pb$_8$Li$_{10}$Cl$_2$(L^{6}H$_2$)$_3$(L^6)(OH)$_2$(O)$_2$(H$_2$O)$_2$(MeCN)$_4$]·14MeCN (2·14MeCN)

L^{6}H$_6$ (1.00 g, 1.03 mmol) and [LiPb(OiPr)$_3$] (0.82 g, 2.04 mmol), generated *in situ* from PbCl$_2$ and LiOiPr, were combined in toluene (20 mL) and the system was refluxed for 12 h. On cooling, the volatiles were removed *in vacuo*, and the residue was extracted into MeCN (20 mL). On standing at 0 °C for 2 days, colourless prisms formed. Yield, 0.79 g, 47%. Anal. calcd for C$_{268}$H$_{323}$Cl$_2$Li$_{10}$N$_2$O$_{30}$Pb$_8$ (sample dried *in vacuo* for 12 h, −16MeCN): C, 55.02; H, 5.57; N, 0.48%; found C, 54.75; H, 5.24; N, 0.79%; IR: 2726w, 2359w, 1645w, 1462s, 1377m, 1364m, 1297w, 1260m, 1203m, 1093m, 1021m, 909w, 872w, 801m, 735m, 527w. ^{1}H NMR (CDCl$_3$) δ: 6.95–7.29 (m, 48H, aryl$H$), 4.56 (d, J = 12 Hz, 12H, −CH$_2$−), 3.98 (d, J = 12 Hz, 12H, −CH$_2$−), 3.46 (d, J = 4.8 Hz, 6H, −CH$_2$−), 3.08–3.18 (m, 18H, −CH$_2$−), 1.97 (s, 18H, MeCN), 1.50 (s, 4H, H_2O), 1.13–1.30 (m, 216H, −C(CH$_3$)$_3$). ^{7}Li (CDCl$_3$) δ: 3.82 (bs), 3.04 (s), 2.83 (bs), 2.61 (bs), 2.41 (bs). ^{207}Pb NMR (C$_6$D$_6$) δ: −2911 (s), −2932 (s), −2957 (s).

Preparation of [Pb$_{13}$(L$^{6'}$)$_3$O$_4$(iPrOH)]·11MeCN (3·11MeCN)

To Pb(OiPr)$_2$ (0.96 g, 2.94 mmol) and L$^{6'}$H$_6$ (0.5 g, 0.49 mmol) was added toluene (30 mL) and the system was refluxed for 12 h. On cooling, the volatiles were removed *in vacuo*, and the residue was extracted into MeCN (30 mL). On standing at room temperature for 3 days, colourless prisms formed. Yield, 0.35 g, 35%. Anal. calcd for C$_{204}$H$_{245}$O$_{28}$Pb$_{13}$ (sample dried *in vacuo* for 12 h, −11MeCN and iPrOH): C, 41.97; H, 4.23%; found C, 42.23; H, 4.54%; IR (nujol mull, KBr): 2726w, 2359w, 1651w, 1539w, 1462s, 1377m, 1260s, 1092s, 1018s, 871s, 799s, 722w. ^{1}H NMR (CDCl$_3$) δ: 6.91–7.62 (m, 36H, aryl$H$), 4.85–5.20 (m, 12H, −OCH$_2$−), 4.45–4.60 (m, 12H, −OCH$_2$−), 4.02–4.22 (m, 12H, −CH$_2$−), 3.39–3.47 (m, 6H, −CH$_2$−), 3.22–3.30 (m, 6H, −CH$_2$−), 1.10–1.32 (m, 162H, −C(CH$_3$)$_3$). ^{207}Pb NMR (C$_6$D$_6$) δ: −2030 (s), −2069 (s), −3301 (bs), −3046 (bs), −3794(s), −3994 (s).

Preparation of [Pb$_{12}$(L^8)$_2$O$_4$]·8.7C$_7$H$_8$ (4·8.7C$_7$H$_8$)

To Pb(OtBu)$_2$ (1.63 g, 4.62 mmol) and L^{8}H$_8$ (1.00 g, 0.77 mmol) was added toluene (30 mL) and the system was refluxed for 3 h. On cooling, the volatiles were removed *in vacuo*, and the residue was extracted into MeCN (30 mL). On standing at 0 °C for 2 days, colourless prisms formed. Yield, 0.68 g, 35%. Anal. calcd for C$_{176}$H$_{208}$O$_{20}$Pb$_{12}$ (sample dried *in vacuo* for 12 h, −8.7C$_7$H$_8$): C, 41.21; H, 4.09%; found C, 41.25; H, 4.50%. IR (nujol mull, KBr): 1685w, 1601w, 1493m, 1362s, 1296s, 1280s, 1260s, 1197s, 1163m, 1117s, 1094bs, 1020bs, 946w, 912w, 899w, 878m, 870m, 817s, 800s, 728s, 702w, 693m, 664w, 634w, 611w, 552w, 528m, 539m, 488m, 475m, 463s. ^{1}H NMR (CDCl$_3$): δ: 6.98–7.34 (m, 16H, aryl$H$), 4.94–5.12 (m, 2H, −CH$_2$−), 4.30–4.40 (m, 4H, −CH$_2$−) 4.13–4.15 (m, 4H, −CH$_2$−), 3.34–3.45 (m, 6H, −CH$_2$−), 1.19–1.27 (m, 72H, −C(CH$_3$)$_3$). ^{207}Pb NMR (C$_6$D$_6$) δ: −2071 (s), −2621 (s). Mass Spec (EI): 2614.7 [M + 2Na$^+$].

Preparation of [Pb$_6$(SiMe$_3$)$_2$(L^8)O$_2$Cl$_2$] (5)

To Pb(N(TMS)$_2$)$_2$ (2.44 g, 4.62 mmol) and L^{8}H$_8$ (1.0 g, 0.77 mmol) was added toluene (30 mL) and the system was refluxed for 12 h. On cooling, the volatiles were removed *in vacuo*, and the residue was extracted into MeCN (30 mL). On standing at 0 °C for 3 days, colourless prisms formed. Yield, 0.71 g, 33%. C$_{94}$H$_{122}$Cl$_2$O$_{10}$Pb$_6$Si$_2$ (sample dried *in vacuo* for 12 h) requires C, 40.58; H, 4.42%; found C, 40.23; H, 4.85%. IR (nujol mull, KBr): 2727w, 2359m, 2341s, 1657w, 1461m, 1414s, 1377m, 1260s, 1200w, 1091s, 1019s, 908w, 867w, 799s, 722w, 703w, 667w. ^{1}H NMR (CDCl$_3$) δ: 6.98–7.24 (m, 16H, aryl$H$), 5.11 (d, J = 12 Hz, 2H, −CH$_2$), 4.87 (m, 4H, −CH$_2$−), 4.47 (m, 4H, −CH$_2$−), 3.97 (d, J = 12 Hz, 2H, −CH$_2$), 3.33 (m, 4H, −CH$_2$−), 1.13–1.34 (m, 72H, −C(CH$_3$)$_3$), 0.07–0.12 (m, 18H, −SiMe$_3$).

^{207}Pb NMR (C$_6$D$_6$) δ: −2918 (s). Mass Spec (EI): 2568.1 [M − 2SiMe$_3$ − 2Cl$^-$].

Preparation of [Pb$_{10}$Li$_2$(L^6)$_2$(OH)Cl(O)$_4$]·9.5MeCN (6·9.5MeCN)

To [Pb(N(TMS)$_2$)$_2$] (1.46 mL, 3.06 mmol), generated *in situ* from hexamethyldisilazane (15.23 mL, 73.58 mmol), *n*BuLi (1.6 M in heptane, 45.99 mL, 73.58 mmol) and PbCl$_2$ (10.23 g, 36.79 mmol) in THF (10 mL), was added L^{6}H$_6$ (0.5 g, 0.51 mmol) in toluene (30 mL) and the system was refluxed for 3 h. On cooling, the volatiles were removed *in vacuo*, and the residue was extracted into MeCN (30 mL). On standing at room temperature for 3 days, colourless prisms formed. Yield, 0.49 g, 46%. C$_{136}$H$_{163}$N$_2$ClLi$_2$O$_{17}$Pb$_{10}$ (sample dried *in-vacuo* for 12 h, −7.5MeCN) requires C, 38.73; H, 3.87; N, 0.66%; found C, 39.11; H, 3.69; N, 0.74%, IR (nujol mull, KBr): 2727w, 2359w, 2340w, 1716w, 1652w, 1505w, 1457s, 1377m, 1260s, 1199w, 1092s, 1018s, 872w, 799s, 722m. ^{1}H NMR (CDCl$_3$) δ: 6.98–7.24 (m, 16H, aryl*H*), 5.23–5.29 (m, 4H, −C*H$_2$*−), 4.65 (d, *J* = 4.8 Hz, 8H, −C*H$_2$*−) 3.91–4.00 (m, 4H, −C*H$_2$*−), 3.47 (d, *J* = 4.8 Hz, 8H, −C*H$_2$*−), 1.99 (s, 6H, MeCN), 1.20–1.35 (m, 108H, −C(C*H$_3$*)$_3$). ^{7}Li (CDCl$_3$): δ = 4.38 (s). ^{207}Pb NMR (C$_6$D$_6$) δ: −2234 (bs), −2525 (bs), −2554 (s), −2874 (bs). Mass Spec (EI): 2056.2 [(M − 9.5MeCN)/2 − Cl$^-$ + Na$^+$].

Preparation of [Pb$_{12}$(L^8)$_2$O$_4$]·12MeCN (7·12MeCN)

The crude (Pb(N(TMS)$_2$)$_2$) product was distilled at 80 °C *in vacuo*.[16] To distilled [Pb(N(TMS)$_2$)$_2$] (2.44 g, 4.62 mmol) and L^{8}H$_8$ (1.0 g, 0.77 mmol) was added toluene (30 mL) and the system was refluxed for 12 h and affording **7** as colourless prisms. Single colourless prisms were grown from a saturated MeCN (30 mL) solution at 0 °C (yield 0.61 g, 31%). Anal. cald for C$_{176}$H$_{206}$O$_{20}$Pb$_{12}$ (sample dried *in vacuo* for 12 h, −12MeCN): anal. cald for C, 41.22 H, 4.05%; found C, 41.62; H, 4.33%. IR (nujol mull, KBr): 2955s, 2853s, 1617w, 1540w, 1462s, 1377m, 1293w, 1259s, 1203s. 1094m, 1019m, 908w, 874w, 817m, 800s, 722w. ^{1}H NMR (C$_6$D$_6$) δ: 6.89–7.46 (m, 16H, aryl*H*), 4.76–4.98 (m, 12H −C*H$_2$*−), 4.22–4.36 (m, 6H, −C*H$_2$*−), 3.27–3.57 (m, 12H, −C*H$_2$*−), 2.95 (d, *J* = 4.8 Hz, 2H, −C*H$_2$*−), 1.29–1.39 (m, 144H, −C(C*H$_3$*)$_3$), ^{207}Pb NMR (C$_6$D$_6$) δ: −2461 (s), −2685 (s), −2861 (s). Mass Spec (EI): 2587.2 [(M − 12MeCN)/2 + Na$^+$].

Procedure for ROP of ε-caprolactone, δ-valerolactone *and rac*-lactide

A toluene solution of pre-catalyst (0.010 mmol, 1.0 mL toluene) was added into a Schlenk tube in the glove-box at room temperature. The solution was stirred for 2 min, and then the appropriate equivalent of BnOH (from a pre-prepared stock solution of 1 mmol BnOH in 100 mL toluene) and the appropriate amount of ε-CL, δ-VL or *r*-LA along with 1.5 mL toluene was added to the solution. The reaction mixture was then placed into an oil/sand bath pre-heated at 130 °C, and the solution was stirred for the prescribed time (8 or 24 h). The polymerization mixture was quenched on addition of an excess of glacial acetic acid (0.2 mL) into the solution, and the resultant solution was then poured into methanol (200 mL).

The resultant polymer was then collected on filter paper and was dried *in vacuo*.

Kinetic studies

The polymerizations were carried out at 130 °C in toluene (2 mL) using 0.010 mmol of complex. The molar ratio of monomer to initiator to co-catalyst was fixed at 500 : 1 : 1, and at appropriate time intervals, 0.5 μL aliquots were removed (under N$_2$) and were quenched with wet CDCl$_3$. The percent conversion of monomer to polymer was determined using ^{1}H NMR spectroscopy.

X-ray crystallography

In all cases, crystals suitable for an X-ray diffraction study were grown from a saturated MeCN solution at either ambient temperature or 0 °C. Single crystal X-ray diffraction data were collected at the UK National Crystallography service using Rigaku Oxford Diffraction ultra-high intensity instruments employing modern areas detectors. In all cases standard procedures were employed for integration and processing of data.

Crystal structures were solved using dual space methods implemented within SHELXT.[21] Completion of structures was achieved by performing least squares refinement against all unique F^2 values using SHELXL-2018[22] sometimes implemented in Olex2. All non-H atoms were refined with anisotropic displacement parameters. Hydrogen atoms were placed using a riding model. Minor disorder was treated using standard methods. SQUEEZE[23] was used to model the disordered solvent in all the structures, except for **4** in which the electron density not associated with the Pb cluster, in two small pockets, was very small and this was not modelled. These are large and complicated structures, but we have been able to identify the atomic arrangements unequivocally. It has not been possible to locate all of the hydrogen atoms (*e.g.* attached to oxygen) but these have been inferred by the need to balance charge.

Conflicts of interest

There are no conflicts to declare.

Acknowledgements

References

1 (*a*) A. Chamas, H. Moon, J. Zheng, Y. Qiu, T. Tabassum, J. H. Jang, M. Abu-Omar, S. L. Scott and S. Suh, *ACS Sustainable Chem. Eng.*, 2020, **8**, 3494–3511; (*b*) M. Labet

and W. Thielemans, *Chem. Soc. Rev.*, 2009, **38**, 3484–3504; (*c*) O. Dechy-Cabaret, B. Martin-Vaca and D. Bourissou, *Chem. Rev.*, 2004, **104**, 6147–6176; (*d*) K. S. Anderson, K. M. Schreck and M. A. Hillmyer, *Polym. Rev.*, 2008, **48**, 85–108; (*e*) K. M. Nampoothiri, N. R. Nair and R. P. John, *Bioresour. Technol.*, 2010, **101**, 8493–8501.

2 (*a*) D. M. Homden and C. Redshaw, *Chem. Rev.*, 2008, **108**, 5086–5130; (*b*) C. Redshaw, *Dalton Trans.*, 2016, **45**, 9018–9030; (*c*) O. Santoro and C. Redshaw, *Coord. Chem. Rev.*, 2021, **448**, 214173–214209.

3 L. Wang, S.-C. Roșca, V. Poirier, S. Sinbandhit, V. Dorcet, T. Roisnel, J.-F. Carpentier and Y. Sarazin, *Dalton Trans.*, 2014, **43**, 4268–4286.

4 L. Wang, S. Fadlallah, C. Bellini, C. Orione, V. Dorcet, J.-F. Carpentier and Y. Sarazin, *Organometallics*, 2015, **34**, 1321–1327.

5 (*a*) T. Xing, T. J. Prior, K. Chen and C. Redshaw, *Dalton Trans.*, 2021, **50**, 4396–4407; (*b*) T. Xing, T. J. Prior, M. R. J. Elsegood, N. V. Semikolenova, I. E. Soshnikov, K. Bryliakov, K. Chen and C. Redshaw, *Catal. Sci. Technol.*, 2021, **11**, 624–636; (*c*) M. J. Walton, S. J. Lancaster, J. A. Wright, M. R. J. Elsegood and C. Redshaw, *Dalton Trans.*, 2014, **43**, 18001–18009; (*d*) M. Frediani, D. Sémeril, A. Mariotti, L. Rosi, P. Frediani, L. Rosi, D. Matt and L. Toupet, *Macromol. Rapid Commun.*, 2008, **29**, 1554–1560.

6 (*a*) A. Bilyk, J. W. Dunlop, A. K. Hall, J. M. Harrowfield, M. W. Hosseini, G. A. Koutsantonis, B. W. Skelton and A. H. White, *Eur. J. Inorg. Chem.*, 2010, 2089–2105; (*b*) R. Kuriki, T. Kuwabara and Y. Ishii, *Dalton Trans.*, 2020, **49**, 12234–12241.

7 (*a*) P. D. Beer, M. G. B. Drew, P. B. Leeson and M. I. Ogden, *J. Chem. Soc., Dalton Trans.*, 1995, 1273–1283; (*b*) F. Arnaud-Neu, G. Barrett, D. Corry, S. Cremin, G. Ferguson, J. F. Gallagher, S. J. Harris, M. A. McKervey and M.-J. Schwing-Weill, *J. Chem. Soc., Perkin Trans. 2*, 1997, 575–580; (*c*) A. F. D. de Namor, S. Chahine, D. Kowaiska, E. E. Castellano and O. E. Piro, *J. Am. Chem. Soc.*, 2002, **124**, 12824–12836; (*d*) N. M. Buie, V. S. Talanov, R. J. Butcher and G. G. Talanova, *Inorg. Chem.*, 2008, **47**, 3549–3558; (*e*) H. J. Kim, S. H. Kim, J. H. Kim, L. N. Anh, J. H. Lee and C.-H. Lee, *Tetrahedron Lett.*, 2009, **50**, 2782–2786; (*f*) M. Bocheńska, J. Kulesza, J. Chojnacki, F. Arnaud-Neu and V. Hubscher-Bruder, *J. Inclusion Phenom. Macrocyclic Chem.*, 2010, **68**, 75–83; (*g*) Y.-Y. Liu, C. Chen, J.-F. Ma and J. Yang, *CrystEngComm*, 2012, **14**, 6201–6214; (*h*) D. Over, X. Zeng, C. Bornholdt, J. Marrot and O. Reinaud, *Inorg. Chem.*, 2013, **52**, 14089–14095; (*i*) B. B. Adhikari, K. Ohto and M. P. Schramm, *Chem. Commun.*, 2014, **50**, 1903–1905; (*j*) E. Lee, Y. Kim, J. Hen and K.-M. Park, *Cryst. Growth Des.*, 2015, **15**, 3556–3560.

8 (*a*) C. Redshaw, *Coord. Chem. Rev.*, 2003, **244**, 45–70; (*b*) S. M. Taylor, S. Sanz, R. D. McIntosh, C. M. Beavers, S. J. Teat, E. K. Brechin and S. J. Dalgarno, *Chem. – Eur. J.*, 2012, **18**, 16014–16022.

9 (*a*) C. Redshaw, D. Homden, D. L. Hughes, J. A. Wright and M. R. J. Elsegood, *Dalton Trans.*, 2009, 1231–1242; (*b*) A. Arbaoui, C. Redshaw, M. R. J. Elsegood, V. E. Wright, A. Yoshizawa and T. Yamato, *Chem. – Asian J.*, 2010, **5**, 621–633.

10 (*a*) J. R. Fulton, P. B. Hitchcock, N. C. Johnstone and E. C. Y. Tam, *Dalton Trans.*, 2007, 3360–3362; (*b*) B. D. Rekken, T. M. Brown, M. M. Olmstead, J. C. Fettinger and P. P. Power, *Inorg. Chem.*, 2013, **52**, 3054–3062.

11 C. Redshaw, M. Rowan, L. Warford, D. M. Homden, A. Arbaoui, M. R. J. Elsegood, S. H. Dale, T. Yamato, C. P. Casas, S. Matsui and S. Matsuura, *Chem. – Eur. J.*, 2007, **13**, 1090–1107.

12 (*a*) Z. Sun, Y. Zhao, O. Santoro, M. R. J. Elsegood, E. V. Bedwell, K. Zahra, A. Walton and C. Redshaw, *Catal. Sci. Technol.*, 2020, **10**, 1619–1639; (*b*) O. Santoro, M. R. J. Elsegood, E. V. Bedwell, J. A. Pryce and C. Redshaw, *Dalton Trans.*, 2020, **49**, 11978–11996.

13 Y. Li, K. Zhao, C. Feng, M. R. J. Elsegood, T. J. Prior, X. Sun and C. Redshaw, *Dalton Trans.*, 2014, **43**, 13612–13619.

14 T. Xing, C. Jiang, M. R. J. Elsegood and C. Redshaw, *Inorg. Chem.*, 2021, DOI: 10.1021/acs.inorgchem.1c02192.

15 O. Santoro, M. R. J. Elsegood, S. J. Teat, T. Yamato and C. Redshaw, *RSC Adv.*, 2021, **11**, 11304–11317.

16 (*a*) Q. Hu, S.-Y. Jie, P. Braunstein and B.-G. Lia, *Chin. J. Polym. Sci.*, 2020, **38**, 240–247; (*b*) M. A. Woodruff and D. W. Hutmacher, *Prog. Polym. Sci.*, 2010, **35**, 1217–1256; (*c*) T. Wu, Z. Wei, Y. Ren, Y. Yu, X. Leng and Y. Li, *Polym. Degrad. Stab.*, 2018, **155**, 173–182; (*d*) M. T. Hunley, N. Sari and K. L. Beers, *ACS Macro Lett.*, 2013, **2**, 375–379; (*e*) Z. Sun, Y. Zhao, O. Santoro, M. R. J. Elsegood, E. V. Bedwell, K. Zahra, A. Walton and C. Redshaw, *Catal. Sci. Technol.*, 2020, **10**, 1619–1639.

17 (*a*) C. Ludwig and M. R. Viant, *Phytochem. Anal.*, 2010, **21**, 22–32; (*b*) M. J. Walton, S. J. Lancaster and C. Redshaw, *ChemCatChem*, 2014, **6**, 1892–1898.

18 (*a*) B. Masci, *J. Org. Chem.*, 2001, **66**, 1497–1499; (*b*) B. Dhawan and C. D. Gutsche, *J. Org. Chem.*, 1983, **48**, 1536–1539.

19 T. Heidemann and S. Mathur, *Eur. J. Inorg. Chem.*, 2014, **3**, 506–510.

20 S. C. Goel, M. Y. Chiang and W. E. Buhro, *Inorg. Chem.*, 1990, **29**, 4640–4646.

21 G. M. Sheldrick, *Acta Crystallogr., Sect. A: Found. Adv.*, 2015, **71**, 3–8.

22 G. M. Sheldrick, *Acta Crystallogr., Sect. C: Struct. Chem.*, 2015, **71**, 3–8.

23 A. L. Spek, *Acta Crystallogr., Sect. C: Struct. Chem.*, 2015, **71**, 9–18.